Title
Feasibility study of a new RF coil design for prostate MRI

Journal
Physics in Medicine and Biology, 59(17)

ISSN
0031-9155

Authors
Ha, Seunghoon
Roeck, Werner W
Cho, Jaedu
et al.

Publication Date
2014-09-07

DOI
10.1088/0031-9155/59/17/n163

Peer reviewed

Feasibility study of a new RF coil design for prostate MRI

Seunghoon Ha[1], Werner W Roeck[1], Jaedu Cho[1], and Orhan Nalcioglu[1]

[1] Tu & Yuen Center for Functional Onco-Imaging, Department of Radiological Sciences, University of California, Irvine, USA

Email: seunghoh@uci.edu

Abstract. The combined use of a torso-pelvic RF array coil and endorectal RF coil is the current state-of-the-art in prostate MRI. The endorectal coil provides high detection sensitivity to acquire high-spatial resolution images and spectroscopic data, while the torso-pelvic coil provides large coverage to assess pelvic lymph nodes and pelvic bones for metastatic disease. However, the use of an endorectal coil is an invasive procedure that presents difficulties for both patients and technicians. In this study, we propose a novel non-invasive RF coil design that can provide both image signal to noise ratio and field of view coverage comparable to the combined torso-pelvic and endorectal coil configuration. A prototype coil was constructed and tested using a pelvic phantom. The results demonstrate that this new design is a viable alternative for prostate MRI

Running Head: New RF coil design for prostate MRI

PACS Codes: 87.61.Ff, 87.61.Tg

Submitted to *Physics in Medicine and Biology*

1. Introduction

In magnetic resonance imaging (MRI), the detection sensitivity of a radiofrequency (RF) loop coil dependents on the distance of the organ to the coil, as well as the coil's shape, size, and orientation. The closer the RF coil is placed to the region-of-interest (ROI), the better the signal-to-noise ratio (SNR) of the resulting MR image (Hayes and Axel 1985). Thus instead of using a general-purpose RF coil (e.g. the cylindrical birdcage coil), dramatic improvements in image quality can be achieved by utilizing an array of loop coils configured for the specific anatomy of interest. The loop coils can be designed and positioned to be as close to the ROI as possible to achieve the maximum SNR.

The torso-pelvic receiver array coil is one such example of tailoring the design for a specific anatomy, in this case the overall pelvic region which includes the prostate. However, the internal position of the prostate, and the distance to the external coils limits its detection sensitivity. As such, prostate MRI using only the torso-pelvic coil lacks sufficient SNR to visualize transcapsular tumor spread or seminal vesicle involvement, resulting in a decrease in staging accuracy and specificity (Fütterer *et al* 2007, Heijmink *et al* 2007). To address the SNR requirements for prostate MRI, an endorectal coil can be utilized instead. This coil is placed internally in close proximity to the prostate, resulting in a substantial increase in the SNR from the prostate. However due to its limited field-of-view (FOV) and non-uniform sensitivity, the endorectal coil can be used in combination with the torso-pelvic coil to provide full coverage of the pelvic region. This approach provides the high SNR of the prostate along with a large FOV to evaluate the pelvic lymph nodes and pelvic bones for metastatic disease. The combination of endorectal and torso-pelvic coils is the current state-of-the-art approach for prostate MRI (Turkbey *et al* 2009).

Despite the improved image quality, the use of an endorectal coil is an invasive, highly uncomfortable procedure that requires a specialized technician to properly position the device and carefully monitor RF heating. Its discomfort for patients and difficulty for technicians poses a significant limitation that impedes the widespread use of prostate MRI. The development of a non-invasive RF coil that provides comparable SNR to the endorectal coil would greatly contribute to the realization of the full clinical potential of prostate MRI. To this end, we investigated the design of a new diaper-shaped array coil (henceforth referred to as the "diaper coil") for significantly improving the image SNR and uniformity of the prostate region. A prototype coil was constructed on an acrylic frame and evaluated by 3T MR imaging of a pelvic phantom. Imaging was also performed using a commercial 6-channel torso-pelvic array coil and single-loop endorectal coil for comparison.

2. Materials and Methods

2.1 Diaper RF Coil Design and Construction

To test the efficacy of this design concept, we constructed and tested a five-segment prototype as shown in figures 1(a-b). The bottom of the array consists of a butterfly-shaped loop coil (width = 80 mm, length = 150 mm) orientated parallel to the x-y plane such that it generates a $\mathbf{B_1}^-$ field along the y-axis. A pair of loop coils (width = 130 mm, length = 80 mm) inclined 12 and 30 degrees about the x-axis were positioned on opposite sides of array to form the diaper shape. The coils were made from copper PCB traces (width = 5 mm, thickness = 34 μm) and positioned with optimum overlap to minimize mutual coupling between adjacent elements (Roemer *et al* 1990).

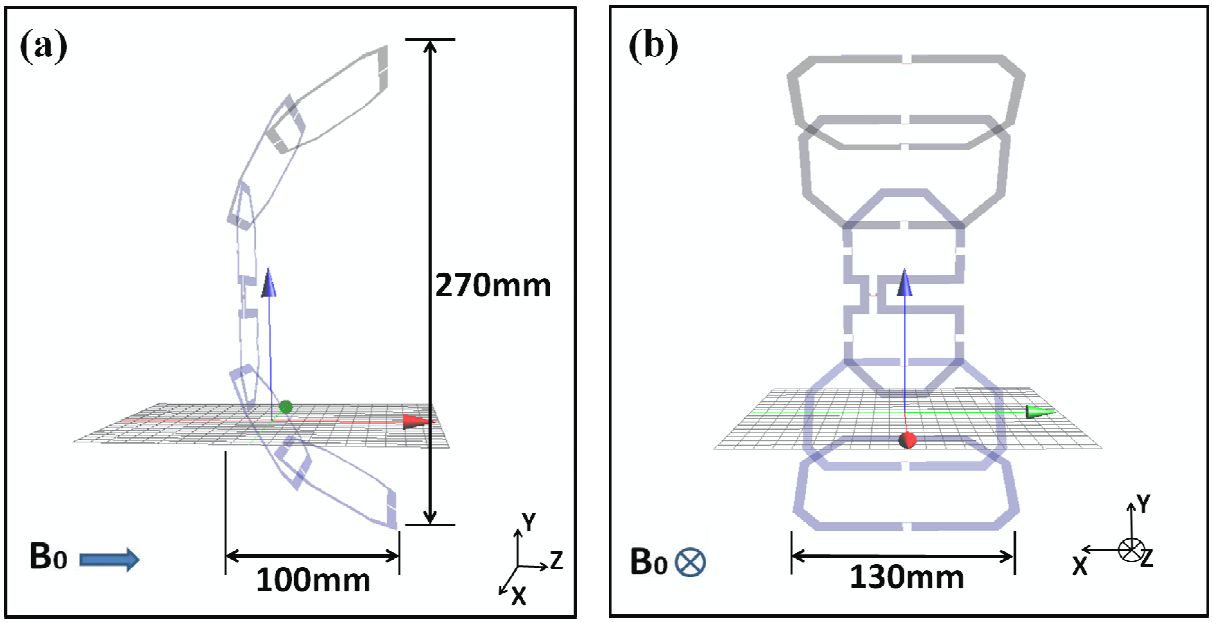

Figure 1. (a) Side view and (b) front view of the diaper coil design.

For constructing the diaper array coil, the circuit pattern for each loop coil was etched on a separate printed circuit board (PCB) composed of flame-retardant G-10 plastic. Discrete capacitors (ATC 100B Series Porcelain Superchip Multilayer Capacitor; American Technical Ceramics Corporation, Huntington Station, USA) and a trimmer capacitor (NMAF30; Voltronics Corporation, Denville, USA) were soldered onto each PCB as shown in figure 2. The individual coils were tuned to 127.7 MHz and the impedance matched to 50 Ω (with phantom loading). Since the array operates in receive-only mode, passive and active detuning circuits containing PIN diodes (UMX9989AP (passive detuning) UM9401 (active detuning); Microsemi, USA) were integrated into the circuit pattern to decouple the coils from the RF transmitter during high power RF transmission. Isolation between adjacent coil elements was measured from the S21 parameters after plugging the two coils to a network analyzer (4395A; Agilent Technologies, USA). After the coil elements were mounted on an acrylic half-cylinder to form the diaper shape, the optimum coil overlap between adjacent coils to reduce mutual coupling was achieved when the isolation measured below -17 dB. The coil elements among non-adjacent coil elements were also decoupled by low noise amplifiers (LNAs: Philips Medical Systems, Netherlands) mounted in a coil interface box (Philips Medical Systems, Netherlands).

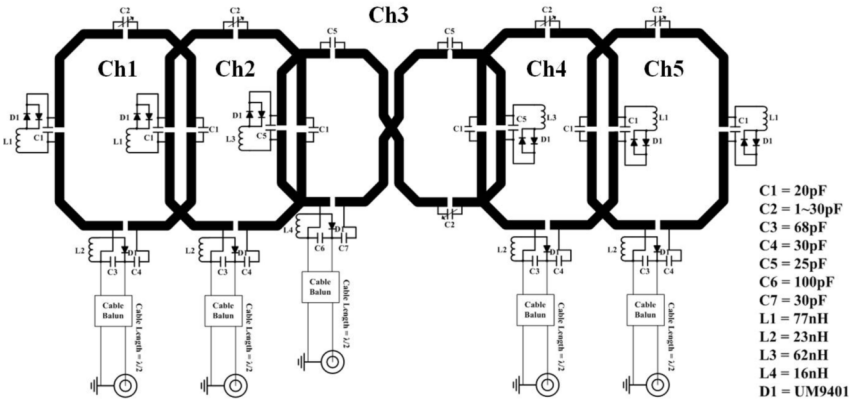

	CH1	CH2	CH3	CH4	CH5
CH1		-18.7	-12.7	-13.1	-15.8
CH2	-18.7		-20.1	-12.0	-14.2
CH3	-12.7	-20.1		-22.5	-13.4
CH4	-13.1	-12.0	-22.5		-19.8
CH5	-15.8	-14.2	-13.4	-19.8	

Unit = (dB)

Figure 2. Circuit diagram of the diaper array coil and isolation measurement table between coil elements.

To interface the array coil with the MRI scanner, we prepared five coaxial cable (length = $\lambda/2$) and connector assemblies each containing a cable balun tuned to 127.7 MHz. For each assembly, one cable end was soldered to the capacitive matching circuit of one coil element and the other end was connected to the coil interface box. Eight LNAs with 25 dB gain, 0.4 dB noise figure, and 5±1 Ω input impedance tuned to 127.7 MHz were also mounted in the coil interface box. Identical LNAs were employed for the torso-pelvic and endorectal coils. The low input impedance of the LNAs effectively work in conjunction with an individual coil's matching/decoupling circuit to eliminate residual magnetic fields induced in neighboring coil elements, thus further reducing mutual coupling. The coil interface box also provided the voltages (-5V) and currents (150 mA) that drive the PIN diode in each active decoupling circuit.

2.2 Experimental Setup

The performance of the diaper coil was compared to a commercial 6-channel torso-pelvic array coil (USA Instruments, Inc.; Aurora, OH) and endorectal coil (Medrad, Inc.; Indianola, PA) though the imaging of an in-house-built pelvic phantom as shown in figures 3. The torso-pelvic coil consists of 6 non-overlapping rectangular loops (width = 125 mm, length = 235 mm). Three loops are placed above the patient, while 3 loops are positioned below the patient, providing coverage of 395 mm along the x-axis and 180 mm along the y-axis. The endorectal coil consists of a single rectangular loop (width = 30 mm, height = 80 mm) formed by a thin copper strip (width = 2 mm, thickness = 34 μm). The pelvic phantom was constructed using acrylic for the oval cylinder (width =300 mm, length = 300 mm, height = 190 mm) to mimic the abdomen and hollow polypropylene balls for the bladder and prostate regions. A hollow polypropylene ball to model the bladder (diameter = 100 mm) and a smaller hollow polypropylene ball to model the prostate (diameter = 35 mm) were positioned within the cylinder to mimic human anatomy (Schulte *et al* 2006, Standring *et al* 2008, Yokochi *et al* 1978).

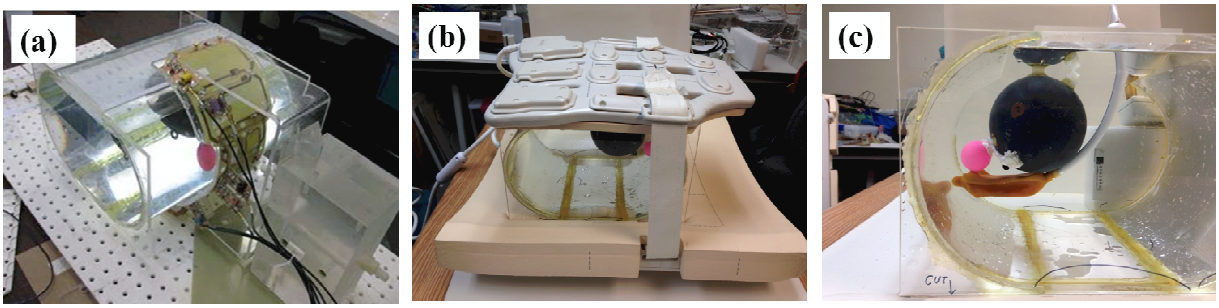

Figure 3. The experimental setup for the proposed coil (a), torso-pelvic coil (b), and endorectal coil (c) using a pelvic/prostate phantom.

To mimic the dielectric properties of the human body, we followed the approach of Yang *et al* (2004), where the concentration of NaCl in solution relative to the phantom volume was adjusted so that the ratio $\sigma/\omega\varepsilon_0\varepsilon_r$ was the same as in human tissue, where ω is the angular (Larmor) frequency and ε_0 is the permittivity of free space. The phantom was filled with 120 mM, 20 mM, and 70 mM of NaCl solution in the abdomen, bladder and prostate regions respectively. 10 mM of $CuSO_4$ was also added to each region to improve image quality in T_1-weighted imaging.

The diaper coil was positioned across the curved face of phantom. The torso-pelvic coil was wrapped on the top and bottom faces of the phantom. The endorectal coil was positioned within the phantom directly underneath the sphere representing the prostate (see figures 3 (a-c)).

2.3 MRI Experiments

MR images of the phantom were acquired using all three coils (diaper, torso-pelvic, endorectal) with a 3T Philips Achieva system (Philips Medical Systems) with the following scan parameters: sequence = T_1-weighted gradient echo, repetition time = 161 ms, echo time = 4.6 ms, flip angle = 80°, matrix = 528 × 528, FOV = 300 mm × 300 mm, slice thickness = 3 mm and number of excitations = 2. Acquired individual coil loop images were combined by most commonly used sum-of-squares algorithm (Roemer *et al* 1990). The axial slice covering the middle of the prostate region was used to calculate the integral uniformity (IU) and the SNR within a local FOV. The SNR of the local FOV was computed by Eq. [1]. The mean signal ($S_{avg.}$) was defined as the mean pixel intensity value in a 50mm ROI covering the prostate phantom. The mean noise ($N_{avg.}$) and the standard deviation (σ) were measured in four regions (20mm square ROI) drawn over an area of no signal (i.e. air) and averaged separately. We avoided measurements on either the phased encoding direction causing ghost artifact or non-uniformities due to bandwidth-limiting filtering (Firbank *et al* 1999).

$$SNR = (S_{avg.}-N_{avg.})/\sigma \qquad \text{Eq. [1]}$$

The percentage integral uniformity (IU) was calculated as Eq. [2] where the maximum and minimum values were taken from pixels within the prostate region.

$$IU = 100 \times \left[\frac{SNR_{max} - SNR_{min}}{SNR_{max} + SNR_{min}} \right] \qquad \text{Eq. [2]}$$

3. Results

MR imaging of the prostate phantom, shown in figures 4(a-f), yielded interesting findings. The measured IU with three different coils were given as 1.2% (Diaper coil), 7.8% (Torso-pelvic coil) and 40.4% (Endorectal coil). It should be emphasized that for a given RF coil, the higher the IU, the worse its uniformity. Both the diaper and torso-pelvic coils provided coverage across the whole phantom while the

endorectal coil was only effective within a very limited FOV. The detection sensitivity in the prostate region was most homogeneous for the diaper coil, followed closely by the torso-pelvic coil, and highly non-uniform for the endorectal coil. In addition, the diaper coil provided significantly higher image SNR than the torso-pelvic coil. While the (non-uniform) SNR of the endorectal coil within the prostate region ranged from 150 to 710, its mean value was comparable to that of the diaper coil (within 8%).

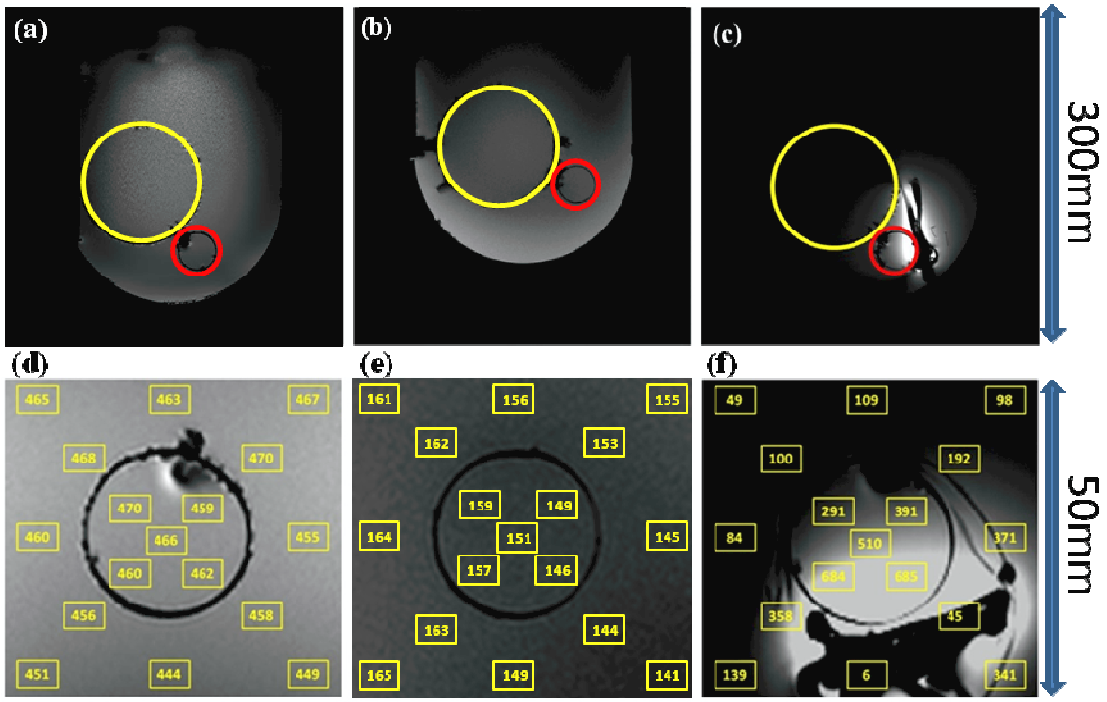

Figure 4. (a-c) Sagittal MR images of the phantom using the (a) diaper, (b) torso-pelvic and (c) endorectal coil. The colored circle areas indicate the bladder phantom (yellow) and the prostate phantom (red). SNR measurements around the prostate region from axial MR slice using the (d) diaper, (e) torso-pelvic and (f) endorectal coil.

4. Discussion

Our results demonstrate that the diaper coil can potentially serve as a noninvasive alternative to the standard torso-pelvic and endorectal coil combination currently used in clinical prostate MRI by providing both comparable image SNR and FOV coverage. While the mean image SNR using the diaper and endorectal coils are similar, the endorectal coil still provides superior detection sensitivity in regions closest to the coil.

Our original 5-channel prototype was designed with the concept of positioning the coil between a patient's legs immediately adjacent to the crotch. The shape of the coil was formed with this configuration in mind, but only tested using phantoms. An *In vivo* study is the essential for further validation of our approach that will be the subject of a future communication. To proceed with *in vivo* studies, a greater attention must be paid to the ergonomics of the coil design. The coil must be designed to fit as comfortable as possible while maintaining its performance quality. Specifically, edges and sharp bends must be shaped to smooth contours, particularly around the patent's crotch. All electronic components must be fully insulated from contact with the patient. The rigid cylindrical acrylic shell used to mount the coil loops can be replaced with flexible, folding elements that can form to each patient's unique body shape.

5. Conclusion

In this note, we proposed a new RF coil design for prostate MRI consisting of a diaper-shaped array of receiver coils placed around the anteroposterior region of the inferior pelvic abdomen and rectum. MRI experiments using a phantom demonstrated that the non-invasive diaper coil can provide image SNR and FOV coverage comparable to the torso-pelvic and invasive endorectal coil combination currently used in clinical practice. This validation justifies further investigation and modification of our design concept to perform imaging on human subjects after receiving appropriate institutional approvals.

Acknowledgements

We thank Dr. Hon Yu for providing the endorectal coil and Dr. Mark Hamamura for editorial assistance.

References

Firbank MJ, Coulthard A, Harrison RM and Williams ED 1999, A comparison of two methods for measuring the signal to noise ratio on MR images. *Phys. Med. Biol.* **44** N261-264

Fütterer J J, Engelbrecht M R, Jager G J, Hartman R P, King B F, Hulsbergen-Van de Kaa C A, Witjes J A and Barentsz JO 2007 Prostate cancer: comparison of local staging accuracy of pelvic phased-array coil alone versus integrated endorectal-pelvic phased-array coils. Local staging accuracy of prostate cancer using endorectal coil MR imaging *Eur. Radiol.* **17** 1055-65

Gabriel S, Lau RW, and Gabriel C 1996 The dielectric properties of biological tissue: III. Parametric models for the dielectric spectrum of tissues *Phys. Med. Biol.* **41** 2271-93

Hayes CE and Axel L 1985 Noise performance of surface coils for magnetic resonance imaging at 1.5 T *Med. Phys.* **12** 604-7

Heijmink S W, Fütterer J J, Hambrock T, Takahashi S, Scheenen T W, Huisman H J, Hulsbergen-Van de Kaa C A, Knipscheer B C, Kiemeney L A, Witjes J A and Barentsz JO 2007 Prostate cancer: body-array versus endorectal coil MR imaging at 3 T--comparison of image quality, localization, and staging performance *Radiology* **244** 184-95

Hoult D I, Chen C N and Snak VJ 1984 Quadrature detection in the laboratory frame *Magn. Reson. Med.* **1** 339-53

Roemer P B, Edelstein W A, Hayes C E, Souza S P and Mueller O M 1990 The NMR phased array *Magn. Reson. Med.* **16** 192-255

Schulte RF, Vogel MW, Schirmer T, Schilling H, Groeger A, and Gross P 2006 Design of an anatomically and physiologically realistic prostate phantom. *Proc. Intl. Soc. Mag. Reson. Med.* 2252

Standring S, Borley NR, Collins P, Crossman AR, Gatzoulis MA, Healy JC, Johnson D, Mahadevan V, Newell RLM, and Wigley CB 2008 Gray's anatomy-The anatomical basis of clinical practice. 4th ed. Spain, Churchill Livingstone 1255-70

Turkbey B, Albert P S, Kurdziel K and Choyke P L 2009 Imaging localized prostate cancer: current approaches and new developments *AJR Am. J. Roentgenol.* **192** 1471-80.

Yang Q X, Wang J, Collins C M, Smith M B, Zhang X, Ugurbil K and Chen W 2004 Phantom design method for high-field MRI human systems *Magn. Reson. Med.* **52** 1016-20

Yokochi C and Rohen JW 1978 Photographic anatomy of the human body. 2nd ed. Baltimore, University Park Press 51-54